Amphipath-Induced Nanoscale Changes in Outer Hair Cell Plasma Membrane Curvature

Jennifer N. Greeson and Robert M. Raphael*
Rice University, Department of Bioengineering, Houston, Texas 77251-1892

ABSTRACT Outer hair cell (OHC) electromotility enables frequency selectivity and sensitivity in mammalian audition. Electromotility is generated by the transmembrane protein prestin and is sensitive to amphipathic compounds including salicylate, chlorpromazine (CPZ), and trinitrophenol (TNP). Although these compounds induce observable membrane curvature changes in erythrocytes, their effects on OHC membrane curvature are unknown. In this work, fluorescence polarization microscopy was applied to investigate the effects of salicylate, CPZ, and TNP on di-8-ANEPPS orientation in the OHC plasma membrane. Our results demonstrate the ability of fluorescence polarization microscopy to measure amphipath-induced changes in di-8-ANEPPS orientation, consistent with nanoscale changes in membrane curvature between regularly spaced proteins connecting the OHC plasma membrane and cytoskeleton. Simultaneous application of oppositely charged amphipaths generally results in no net membrane bending, consistent with predictions of the bilayer couple hypothesis; however, the application of salicylate (10 mM), which inhibits electromotility, is not reversed by the addition of CPZ. This result supports other findings that suggest salicylate primarily influences electromotiliy and OHC nonlinear capacitance via a direct interaction with prestin. In contrast, we find that CPZ and TNP influence the voltage sensitivity of prestin via membrane bending, demonstrating the mechanosensitivity of this unique membrane motor protein.

INTRODUCTION

Outer hair cells (OHCs) of the mammalian cochlea respond to changes in transmembrane potential via whole-cell, axial deformations (1–3), a process referred to as electromotility. Electromotility contributes to the sensitivity and frequency selectivity of mammalian hearing (4–6) and is often characterized by its accepted electrical signature, a measurable, voltage-dependent nonlinear capacitance (NLC) (7). This NLC represents charge movement within the OHC membrane, similar to an ion channel gating current, that is tightly coupled to voltage-driven length changes (8–10). The dependence of this capacitance on transmembrane potential follows a bell-shaped curve, the peak of which occurs at the voltage where the highest electromotile gain is realized. Several perturbations are known to affect the NLC operating range, including membrane tension (11); membrane cholesterol concentration (12,13); and exposure to the amphipathic compounds salicylate (14,15), chlorpromazine (CPZ) (16,17), and trinitrophenol (TNP) (17). Each of these amphipath-induced perturbations results in a depolarizing shift in NLC voltage dependence; however, in the case of 10 mM salicylate, NLC and electromotility are almost entirely abolished (14,15,18). The biophysical mechanism(s) responsible for these effects are unknown, but salicylate and CPZ have been reported to affect lipid lateral mobility (19) and OHC plasma membrane mechanical properties (20,21), and these compounds have corresponding effects on two physiological measures of hearing: the compound action potential and distortion product otoacoustic emissions (22).

The effects of amphipathic compounds on cell membrane mechanics were originally documented in classic studies conducted in red blood cells (RBCs), which formed the basis for the bilayer couple hypothesis of membrane shape transitions (23–25). Compounds that are negatively charged, such as salicylate and TNP, partition preferentially into the outer bilayer leaflet, generating leaflet expansion and outward membrane bending. Positively charged amphipaths, including CPZ, partition into the negatively charged inner leaflet and generate inward membrane bending. The manifestation of this preferential partitioning is demonstrated by images of RBCs that are crenulated when exposed to salicylate or TNP or cupped when exposed to CPZ (26). Quantitative models based on area-difference elasticity (27) were developed and later used to explain a range of RBC shape transitions (28–30), further refining the bilayer couple hypothesis.

The molecular basis for OHC electromotility and NLC is the transmembrane protein prestin (6,31). Prestin is a member of the SLC26 superfamily of anion transporters (32) and is expressed highly and selectively in the plasma membrane of OHCs (33). Models for the role of a motor protein in electromotility predict that the protein undergoes conformational changes within the plane of the membrane (34–37) or in a manner that coincides with or induces membrane bending (38). The models purport that the concerted action of many densely packed protein molecules translates to whole-cell axial deformations.

Evidence that the plasma membrane can act as an allosteric modulator of transmembrane protein function is mounting (39), and membrane perturbations that affect prestin function such as modulation of membrane cholesterol

Submitted May 5, 2008, and accepted for publication September 24, 2008.

*Correspondence: rraphael@rice.edu

Editor: Denis Wirtz

0006-3495/09/01/0510/11 $2.00

doi: 10.1016/j.bpj.2008.09.016

(13), tension (11), or the introduction of amphipaths (14–17) are likely linked to alterations of prestin-membrane interactions. Bilayer couple effects have been well characterized in mechanosensitive ion channels (40,41), and membrane curvature stress has been shown to affect the function of many proteins, including rhodopsin (42) and the Ca^{2+}-activated BK channel (43,44). Additionally, membrane curvature has been predicted (45) and demonstrated (46) to affect protein oligomerization, a finding made more relevant to the auditory field following the demonstration of prestin self-association (47–50). Changes in curvature can result from alterations in the membrane lateral pressure profile, which is highly dependent on membrane composition and influences the work associated with protein conformational changes (51–55), such as those predicted for prestin. Lateral pressure profile effects are more pronounced for proteins with depth-dependent cross sectional areas. Interestingly, a recent electron microscopy study indicates that prestin is a bullet-shaped molecule with a greater cross sectional area in the membrane's inner leaflet (56).

Given the effects of amphiphiles on RBC shape and the apparent mechanosensitivity of prestin, it is reasonable to postulate that salicylate, CPZ, and TNP exert their influence on prestin function and electromotility through modulation of membrane curvature. However, understanding these effects requires consideration of the unique architecture and mechanics of the OHC lateral wall, which contains three structures: the plasma membrane, a cortical cytoskeleton, and the subsurface cisternae. Specifically, the OHC cortical cytoskeleton is made up of circumferentially wound actin filaments cross-linked by spectrin filaments oriented along the longitudinal axis of the cell (57,58). An additional structure of unknown molecular identity, visible in electron micrographs, connects the plasma membrane to the cytoskeleton at fairly regularly spaced intervals both in the axial and circumferential direction. This structure, referred to as the pillar protein, has been postulated to provide necessary anchor points that allow the OHC plasma membrane to bend in a consistent and regular manner (38). The cortical cytoskeleton and a positive intracellular (turgor) pressure together help maintain the cylindrical shape of the OHC and greatly influence overall cell mechanics (5,57,59). Although previous models have predicted OHC plasma membrane bending between pillar attachment sites, it remains controversial whether the membrane is free to deform in this manner or instead remains tightly coupled to the underlying cytoskeleton, as discussed in recent reviews (4,7).

To investigate the hypothesis that amphipathic compounds induce OHC plasma membrane bending, we employed fluorescence polarization microscopy (FPM), a quantitative microscopy technique capable of measuring fluorophore orientation with respect to the plane of the membrane. We recently developed FPM for use in the quasicylindrical OHC and demonstrated its ability to measure the orientation of pyridinium, 4-[2-[6-(dioctylamino)-2-naphthalenyl]ethenyl]-1-(3-sulfopropyl) (di-8-ANEPPS) in the plasma membrane (60). This novel implementation of FPM required a reformulation of the original theory developed by Axelrod for use in sphered RBCs (61). Di-8-ANEPPS is a voltage-dependent probe designed to partition into the membrane and align with the polar and nonpolar regions of adjacent lipids (62,63). In previous studies of di-8-ANEPPS orientation in the OHC, we found that its absorption transition dipole moment maintains an orientation of ~27° with respect to the plane of the membrane, corresponding to an emission transition dipole moment orientation of ~89° (60). Because of this orientation parallel to the acyl chains of the membrane lipid component, we predicted that di-8-ANEPPS would be a sensitive indicator of changes in membrane curvature.

In this work, FPM is employed to investigate the effects of curvature-inducing amphipaths on the orientation of di-8-ANEPPS with respect to the OHC plasma membrane. A model of OHC plasma membrane bending is then invoked to explain observed orientation shifts. Measured changes in di-8-ANEPPS orientation are consistent with changes in nanoscale membrane curvature and suggest that CPZ and TNP exert their effects on prestin through changes in membrane curvature. Conversely, salicylate's competition with intracellular anions necessary for prestin function (64,65) may dominate any membrane-mediated effects and explain salicylate's ability to diminish NLC rather than simply shift the voltage dependence of the NLC.

MATERIALS AND METHODS

Outer hair cell isolation, loading, and treatment

OHCs were isolated from female albino guinea pigs weighing 150–225 g, as described previously (60). Animals were anesthetized with halothane before decapitation. Temporal bones were placed in standard extracellular bathing solution (140 mM NaCl, 5 mM KCl, 10 mM HEPES, 10 mM glucose, 1 mM $MgCl_2$, 2 mM $CaCl_2$, ~290–300 mOsm, pH 7.3), and the otic capsule was removed up to the second cochlear turn. The entire temporal bone was then placed in extracellular solution containing 150 μM di-8-ANEPPS and incubated at room temperature for 20 min. Following dye loading, OHC isolation was carried out in one of seven amphipath-containing solutions. Cells were exposed to either 0.5 mM salicylate, 10 mM salicylate, 0.1 mM CPZ, 0.1 mM TNP, 0.5 mM salicylate and 0.1 mM CPZ simultaneously, 10 mM salicylate and 0.1 mM CPZ simultaneously, or 0.1 mM CPZ and 0.1 mM TNP simultaneously. All solutions were adjusted to pH 7.3 and ~290–300 mOsm (with glucose). Following suspension in the amphipath-containing solutions, FPM images were collected after 10 min but within 1.5 h after amphipath introduction.

Outer hair cell fluorescence polarization microscopy

FPM experiments were implemented as described previously using a Zeiss Axiovert 200M fluorescence microscope, a Plan-Apochromat 63×, NA 1.4 objective lens, and a cooled charged-coupled device camera (Axiocam) (Carl Zeiss Microimaging, Thornwood, NY) (60). Briefly, OHCs were selected for imaging using standard OHC selection criteria. Cells maintained a uniform cylindrical shape, had a nucleus showing little axial migration, and exhibited minimal internal Brownian motion. Cells fitting these criteria were brought into vertical alignment with the optical axis, and two FPM

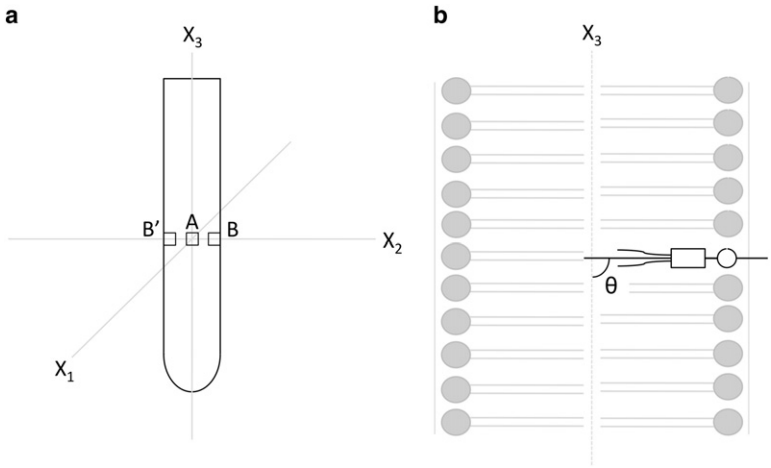

FIGURE 1 (*a*) Orientation of an OHC in the fixed, microscope frame of reference denoted by the X coordinate system. The regions A, B, and B′ are the FPM measurement regions. The orientation of the emission polarizer is defined as parallel when its transmission axis is aligned along the X_3 axis and defined as perpendicular when its transmission axis is aligned along the X_2 axis. (*b*) Schematic representing the orientation of di-8-ANEPPS (shown in *black*) in the membrane. The angle θ defines fluorophore orientation with respect to the X_3 axis, or the plane of the uncurved membrane.

images were obtained. The first image uses parallel excitation and emission polarizations, and the second preserves the excitation polarization direction but uses a crossed emission polarizer. Intensity measurements from three regions of interest (Fig. 1 *a*) were obtained for FPM analysis and optimization. Before imaging each day, necessary calibration factors were obtained and remained within the range previously published (60).

From intensity measurements, five ratios are calculated (Eq. 1). Here the subscript denotes the orientation of the emission polarizer, and the superscript denotes the measurement region. The measurement taken at the left side of the cell (B′) is averaged with the intensity at point B to exploit the natural symmetry of the OHC.

$$\frac{F_{\perp}^{B}}{F_{\parallel}^{B}}, \frac{F_{\parallel}^{A}}{F_{\parallel}^{B}}, \frac{F_{\perp}^{A}}{F_{\perp}^{B}}, \frac{F_{\perp}^{A}}{F_{\parallel}^{B}}, \frac{F_{\perp}^{B}}{F_{\parallel}^{A}} \tag{1}$$

These ratios can also be theoretically predicted, as described previously (60), and optimization between the measured and predicted values depends upon the orientation of the fluorophore, defined as θ, and the percentage of molecules that maintain this orientation, the oriented fraction (OF). Optimization is carried out using MATLAB's (The Mathworks, Natick, MA) built-in genetic algorithm toolbox, as described previously (60). The value θ represents the orientation of the absorption transition dipole moment of di-8-ANEPPS with respect to the plane of the membrane brought into alignment with the optical axis X_3 (Fig. 1 *b*).

For all treatment groups, the resulting θ, OF, and fitting function value (ffval) are presented. In the course of experimentation, we found the ratio $F_{\perp}^{B}/F_{\parallel}^{A}$ to be an excellent indicator of di-8-ANEPPS internalization, a sign of degraded OHC health. The fluorescence from the center region A should always be low compared to the membrane region B, particularly with a perpendicular analyzer. If this ratio is less than or equal to one for any cell, di-8-ANEPPS has been internalized, and the cell is removed from the final cell pool to prevent confounding of FPM intensity measurements.

FPM was used to investigate the orientation of di-8-ANEPPS in OHCs treated with various amphipathic compounds known to alter membrane curvature. OHCs were exposed to either a positively charged, inward bending amphipath (CPZ) or a negatively charged, outward bending amphipath (salicylate, TNP) for individual treatments. For dual treatments, CPZ was paired with one of the negatively charged amphipaths to neutralize membrane bending. Amphipath treatments of OHCs did not result in visible morphological changes such as those seen in RBCs (Fig. 2), consistent with earlier reports (17,19–22). It has previously been documented that OHCs undergo a shortening when exposed to CPZ and TNP (17); however, we did not assess length changes as OHCs were visualized only after treatment with amphipathic compounds.

A total of 83 OHCs was analyzed for this study. Control results from a previously published study were reinterpreted using the restriction described above for $F_{\perp}^{B}/F_{\parallel}^{A}$, allowing comparison to new data (60). All experimental conditions for treatment groups are consistent with those used to obtain the control cell pool allowing this comparison. Two methods were used to determine θ and OF. In the first, referred to as grouped, the average ratio values for each treatment case were used for optimization. In the second, referred to as individual, the FPM optimization algorithm is carried out for each individual cell's ratio values, and the resulting θ and OF values are averaged to represent the entire cell pool. A comparison of these results demonstrates consistency between the methods (Table 1); however, we will restrict our discussion to the individual averaged orientations since they allow statistical comparison between treatment groups and control.

Statistical analysis

Statistical analysis was conducted using a one-factor (amphipath treatment) analysis of variance for all groups. This analysis was carried out for both θ and OF individually. If a parameter's F-test was significant ($p < 0.05$), a Tukey's post hoc analysis was completed. The *p*-values subsequently referred to were generated from these post hoc analyses.

RESULTS

The cells shown in Fig. 2 are representative of all cells from each treatment group throughout the course of the study. Though alterations in OHC plasma membrane architecture were not readily apparent from FPM images, changes in OHC FPM ratios were evident between treatment groups (Table 1).

Outer hair cell treatment with CPZ and TNP

In untreated OHCs, the orientation of di-8-ANEPPS is 29.9° ± 8.6° with respect to the plane of the membrane. In cells treated with 0.1 mM TNP, di-8-ANEPPS orients at 13.3° ± 5.6° corresponding to a significant shift of 16.6° ($p < 0.001$). In cells treated with 0.1 mM CPZ, di-8-ANEPPS orients at 18.3° ± 5.1°, shifted 11.6° from the control orientation ($p < 0.05$) (Fig. 3 and Table 1). Interestingly, in cells treated simultaneously with CPZ and TNP (both at 0.1 mM), di-8-ANEPPS orients at 23.3° ± 6.5°, which is not statistically significantly different from the control orientation. This result suggests that CPZ and TNP are capable of attenuating each other's bending effects (Fig. 4 and Table 1).

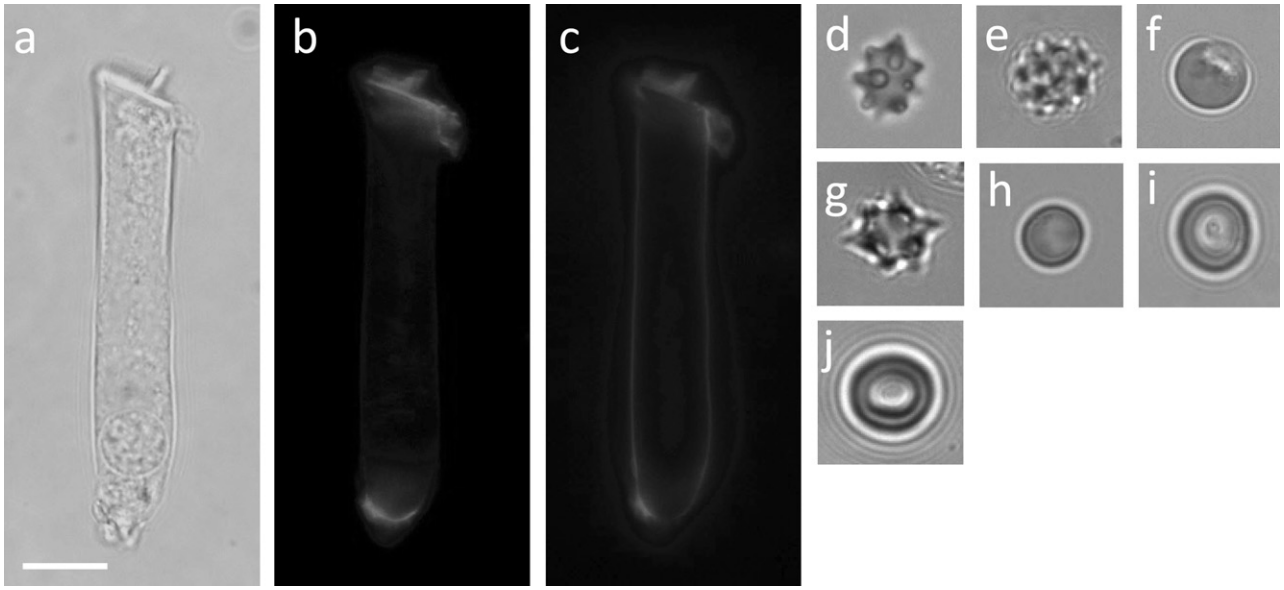

FIGURE 2 OHC FPM images. (*a–c*) These sample images from a cell treated with 10 mM salicylate are representative of images obtained from all amphipath treatment groups. As shown here, no visible, morphological changes were seen in OHCs treated with amphipaths. (*a*) Transmitted light image. Scale bar is 10 μm. (*b*) FPM image obtained with parallel excitation and emission polarizers. (*c*) FPM image obtained with crossed excitation and emission polarizers. (*d–j*) Transmitted light images of RBCs from each amphipath treatment group. These images are included to demonstrate that RBCs included in OHC treatment dishes underwent shape transitions as expected. Images are of RBCs treated with (*d*) 0.5 mM salicylate, (*e*) 10 mM salicylate, (*f*) 0.1 mM CPZ, (*g*) 0.1 mM TNP, (*h*) 0.5 mM salicylate and 0.1 mM CPZ simultaneously, (*i*) 10 mM salicylate and 0.1 mM CPZ simultaneously, and (*j*) 0.1 mM TNP and 0.1 mM CPZ simultaneously.

No significant differences are reported in the OFs corresponding to each treatment group (Table 1).

Outer hair cell treatment with salicylate

Two different concentrations of salicylate were investigated in both individual and dual treatments. Among all amphipaths studied, salicylate alone has the ability to almost completely block NLC and electromotility at 10 mM, but this block is reversible (14,15,18). At lower concentrations (0.5 mM), salicylate attenuates NLC and electromotility (15) while inducing a similar depolarizing shift in the operating range, as reported with CPZ and TNP (17). Thus, we investigated salicylate's effects on di-8-ANEPPS orientation at both 10 mM and 0.5 mM.

Di-8-ANEPPS maintained an average orientation of $21.0^\circ \pm 8.5^\circ$ with respect to the plane of the membrane in OHCs treated with 0.5 mM salicylate. This reduction in orientation angle from the control group is not statistically significant ($p = 0.11$). Treatment with 10 mM salicylate reduces the orientation angle further to $18.5^\circ \pm 6.9^\circ$ ($p < 0.05$) (Fig. 3 and Table 1). Dual treatment with 0.5 mM salicylate and 0.1 mM CPZ results in a di-8-ANEPPS orientation of $24.0^\circ \pm 9.2^\circ$, statistically similar to the control orientation ($p = 0.73$). However, dual treatment with 10 mM salicylate and 0.1 mM CPZ results in a di-8-ANEPPS orientation of $16.0^\circ \pm 7.7^\circ$ ($p < 0.005$) (Fig. 4 and Table 1). No significant shifts in the OF are observed for salicylate treatment cases (Table 1).

DISCUSSION

We have demonstrated the ability of FPM to detect shifts in the orientation of di-8-ANEPPS in OHCs exposed to membrane curvature-inducing amphipaths. Di-8-ANEPPS was chosen for these experiments for two reasons. First, this fluorophore has been used successfully in numerous quantitative fluorescence microscopy studies in the OHC (19,60,66–68). These studies demonstrated that di-8-ANEPPS partitions effectively and selectively into the OHC plasma membrane and is not significantly internalized in healthy, excised cells during the time course of FPM experimentation. Second, di-8-ANEPPS was chosen for its preferred orientation in the plasma membrane. Predictions based on chemical structure and our previous measurement of di-8-ANEPPS orientation in untreated OHCs (60) indicate the molecule partitions with the long axis of its chromophore parallel to the long axis of adjacent lipids (Fig. 1). As the molecule will remain in the completely extended trans state during experimentation (62), the probe should behave as a rigid indicator of membrane curvature. Additionally, because the structure of the fluorophore mimics that of its lipid counterparts, minimal perturbations to the membrane environment are expected to result from its incorporation into the plasma membrane (62).

OHCs labeled with di-8-ANEPPS were treated with three different amphipathic compounds in a series of individual and dual treatments to test for bilayer couple effects. None of these treatments resulted in visible morphological changes in OHC plasma membrane shape; however, all individual

TABLE 1 FPM optimization results for all treatment groups

	Control ($n = 13$)		0.1 mM TNP ($n = 8$)		0.1 mM CPZ ($n = 10$)		0.1 mM TNP + 0.1 mM CPZ ($n = 12$)	
Ratio	Experiment	Theory	Experiment	Theory	Experiment	Theory	Experiment	Theory
$F^B_\perp/F^B_\parallel$	1.44 ± 0.19	1.46	1.17 ± 0.09	1.16	1.22 ± 0.08	1.21	1.28 ± 0.16	1.34
$F^A_\parallel/F^B_\parallel$	1.02 ± 0.07	0.88	1.02 ± 0.04	0.86	1.02 ± 0.02	0.89	1.04 ± 0.04	0.89
$F^A_\perp/F^B_\perp$	0.63 ± 0.11	0.69	0.72 ± 0.09	0.84	0.74 ± 0.06	0.84	0.66 ± 0.11	0.76
$F^A_\perp/F^B_\parallel$	0.89 ± 0.12	1.01	0.83 ± 0.07	0.97	0.90 ± 0.03	1.02	0.84 ± 0.09	1.02
$F^B_\perp/F^A_\parallel$	1.41 ± 0.20	1.64	1.14 ± 0.09	1.35	1.20 ± 0.06	1.37	1.23 ± 0.16	1.51
	$\theta_{grouped}$	29.7°	$\theta_{grouped}$	14.0°	$\theta_{grouped}$	19.2°	$\theta_{grouped}$	26.1°
	$OF_{grouped}$	46.0%	$OF_{grouped}$	69.0%	$OF_{grouped}$	52.3%	$OF_{grouped}$	45.5%
	ffval	0.62	ffval	1.77	ffval	1.96	ffval	1.69
	$\theta_{individual}$	29.9° ± 8.6°	$\theta_{individual}$	14.0° ± 5.7°**	$\theta_{individual}$	18.3° ± 5.1°*	$\theta_{individual}$	23.0° ± 6.3°
	$OF_{individual}$	47.9% ± 18.6%	$OF_{individual}$	72.8% ± 12.5%	$OF_{individual}$	55.0% ± 9.6%	$OF_{individual}$	51.3% ± 17.7%
	0.5 mM Salicylate ($n = 9$)		10 mM Salicylate ($n = 10$)		0.5 mM Salicylate + 0.1 mM CPZ ($n = 6$)		10 mM Salicylate + 0.1 mM CPZ ($n = 10$)	
Ratio	Experiment	Theory	Experiment	Theory	Experiment	Theory	Experiment	Theory
$F^B_\perp/F^B_\parallel$	1.26 ± 0.12	1.28	1.21 ± 0.09	1.21	1.50 ± 0.23	1.47	1.16 ± 0.05	1.17
$F^A_\parallel/F^B_\parallel$	1.04 ± 0.04	0.86	1.03 ± 0.04	0.87	1.03 ± 0.06	0.81	1.05 ± 0.03	0.91
$F^A_\perp/F^B_\perp$	0.67 ± 0.05	0.76	0.72 ± 0.05	0.82	0.56 ± 0.13	0.62	0.79 ± 0.03	0.89
$F^A_\perp/F^B_\parallel$	0.85 ± 0.06	0.98	0.87 ± 0.06	0.99	0.81 ± 0.06	0.92	0.92 ± 0.05	1.04
$F^B_\perp/F^A_\parallel$	1.22 ± 0.09	1.49	1.18 ± 0.07	1.39	1.45 ± 0.26	1.80	1.11 ± 0.04	1.29
	$\theta_{grouped}$	21.6°	$\theta_{grouped}$	18.5°	$\theta_{grouped}$	25.9°	$\theta_{grouped}$	15.5°
	$OF_{grouped}$	57.0%	$OF_{grouped}$	57.8%	$OF_{grouped}$	62.2%	$OF_{grouped}$	53.71%
	ffval	2.03	ffval	1.75	ffval	1.34	ffval	2.11
	$\theta_{individual}$	21.0° ± 8.5°	$\theta_{individual}$	18.5° ± 6.9°*	$\theta_{individual}$	24.0° ± 9.2°	$\theta_{individual}$	16.0° ± 7.7°**
	$OF_{individual}$	60.8 ± 17.6%	$OF_{individual}$	58.9% ± 18.8%	$OF_{individual}$	67.7% ± 13.3%	$OF_{individual}$	55.7% ± 23.9%

Theoretical FPM ratio values were obtained using average ratio values for each treatment group.
*$p < 0.05$.
**$p < 0.005$.

treatments shifted di-8-ANEPPS orientation as measured by changes in θ, and, with the exception of 0.5 mM salicylate, these shifts were statistically significant (Fig. 3 and Table 1). Treatments of OHCs with two amphipaths simultaneously were also conducted. When 10 mM salicylate was simultaneously applied with 0.1 mM CPZ, the orientation of di-8-ANEPPS remained significantly shifted. However, when either 0.1 mM TNP and 0.1 mM CPZ or 0.5 mM salicylate and 0.1 mM CPZ were applied together, the measured orientation of di-8-ANEPPS was statistically equivalent to that in untreated cells. These latter results suggest that CPZ and TNP qualitatively follow the predictions of the bilayer couple hypothesis in the OHC. By partitioning into opposing leaflets, CPZ and TNP diminish the differential area expansion that drives curvature changes when the compounds are applied individually. CPZ also seems capable of partially attenuating salicylate's effect on di-8-ANEPPS orientation at low salicylate concentrations, though the differences between the individual and dual treatment are not statistically significantly different according to rigorous statistical analyses.

Membrane curvature model of di-8-ANEPPS reorientation

The data presented here document the reorientation of the membrane probe di-8-ANEPPS following treatment of OHCs with salicylate, CPZ, and TNP. These amphipathic compounds cause curvature-induced shape transformations in RBCs; however, despite theoretical predictions (17,19,38), experiments had not previously determined whether such membrane curvature changes are manifested in OHCs. Before

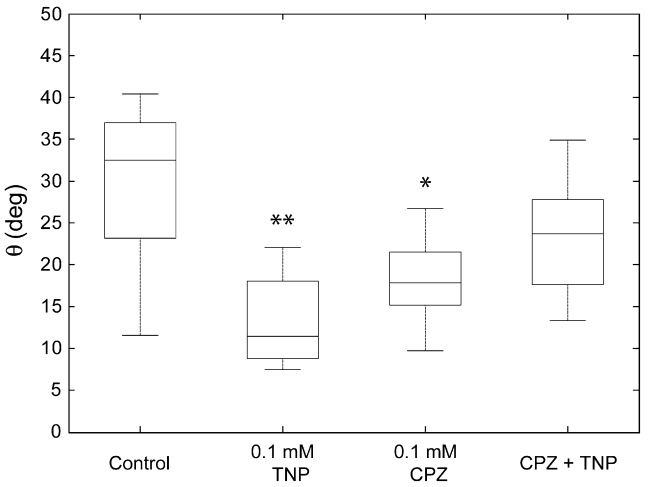

FIGURE 3 Di-8-ANEPPS orientations for cells treated with CPZ and TNP. Box ends designate the upper and lower quartiles of the data. Medians are shown as lines through each box and whiskers indicate the extent of the data up to 1.5 times the standard deviation. Averages and standard deviations for each group are presented in Table 1 (*$p < 0.05$, **$p < 0.005$).

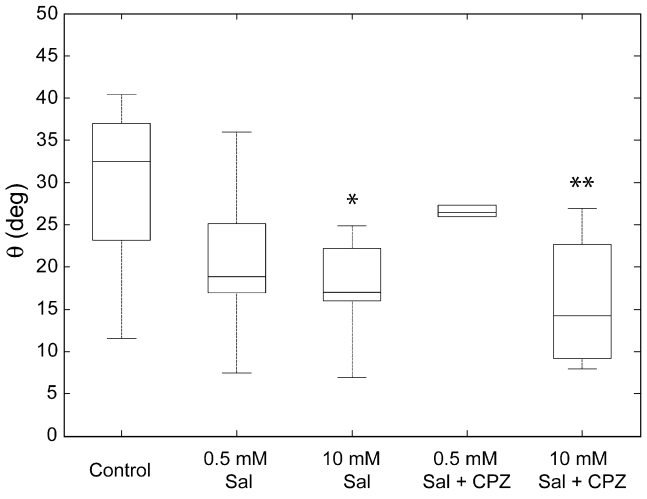

FIGURE 4 Di-8-ANEPPS orientations for cells treated with CPZ and TNP. As with Fig. 2, box ends designate the upper and lower quartiles of the data. Medians are shown as lines through each box, and whiskers indicate the extent of the data to 1.5 times the standard deviation. In the case of simultaneous treatment with 0.5 mM salicylate and CPZ, the tightening of the distribution is explained by the presence of two outliers. Averages and standard deviations for each group are presented in Table 1 (**$p < 0.005$).

answering this question, we first examine potential mechanisms for the induced shifts in di-8-ANEPPS orientation. Since both di-8-ANEPPS and the amphipathic compounds used partition into the plasma membrane, the potential exists for molecular interactions that may confound orientation measurements. We rule out this possibility as follows. First, if CPZ and TNP only exerted their effects on di-8-ANEPPS orientation through a molecular or electrostatic interaction, the simultaneous application of the two compounds would not result in a return to the control orientation. Instead, the measured orientation of di-8-ANEPPS would be a weighted average of the two orientations found when cells are treated with each compound individually.

Additionally, we have investigated the effects of both 10 and 50 mM salicylate on the orientation of di-8-ANEPPS in 1-stearoyl-2-oleoyl-*sn*-glycero-3-phosphatidylcholine (SOPC) giant unilamellar vesicles (69) using methods presented previously (70). In these studies, even at 50 mM, salicylate only induced a di-8-ANEPPS orientation shift of ~2°. Although this may indicate a small amount of interaction between salicylate and di-8-ANEPPS, it cannot account for the much larger shifts in di-8-ANEPPS orientation seen in OHCs. This is also an important finding, as the lack of di-8-ANEPPS orientation shift in amphipath-treated giant unilamellar vesicles confirms the necessity of leaflet charge asymmetry in driving preferential partitioning of amphipathic compounds. In a pure SOPC membrane without a negatively charged inner leaflet, salicylate would partition more easily into both leaflets. In the absence of preferential partitioning, no changes in membrane curvature would be expected, though the mechanical properties of the membrane would still be affected as shown previously (71).

It could also be argued that the reversal of di-8-ANEPPS orientation shifts in the dual treatment cases results from a direct interaction between the positively and negatively charged amphipaths in solution. This is unlikely, however, as this interaction would occur rather quickly in solution and would result in the formation of a readily visible precipitate, something not seen during experimentation. We are thus led to conclude that the measured changes in di-8-ANEPPS orientation reflect changes in OHC plasma membrane curvature.

The membrane curvature model described here, similar to those that have come before it (17,19,38), presumes that the membrane is ''pinned'' by cytoskeletal pillar proteins but is capable of deformation in the regions between these anchor points (Fig. 5). We first determined a two-dimensional relationship between pillar spacing and deformation. In Fig. 5, the plane of the membrane is represented by the dark gray line, and oriented di-8-ANEPPS molecules are shown as light gray arrows. The transition from Fig. 5, *a* to *b*, indicates the allowed deformation of the membrane. On the deformed arc, the orientation at point B represents the average orientation for all di-8-ANEPPS molecules, assuming an even distribution along the length of the curve. We rely on this assumption for simplicity, recognizing that our model does not account for complex curvatures that may arise at the intersection of the pillar and the plasma membrane. It is conceivable, however, that di-8-ANEPPS avoids these regions due to crowding or hydrophobic mismatch at the protein interface and instead favors the membrane arc as modeled.

If we assume that the measured orientation shifts correspond to the ensemble orientation represented by point B along a region of curved OHC membrane, we can calculate the corresponding angle that subtends the membrane arc (δ) (Fig. 5 *b*). Values for δ that correspond to measured orientation shifts ($\Delta\theta$) are shown in Table 2. A simple geometric equation relates δ, the arc length (s), the radius of curvature (r_c), and the pillar spacing (p) and is shown in Eq. 2.

$$s = r_c\delta,$$

where

$$\delta = 2\sin^{-1}\left(\frac{p}{2r_c}\right). \quad (2)$$

Using Eq. 2, we can plot the relationship between these parameters over a range of relevant values. The spacing between pillar proteins is estimated to range from 20 to 80 nm (58), and our own observations using electron tomography (W. J. Triffo, R. M. Raphael, and M. Auer, unpublished) suggest an axial pillar spacing of ~36 nm which agrees with previous measurements (72). Reasonable bounds for the radius of curvature are 10–100 nm. In Fig. 5 *c*, we show the relationship between these parameters and our measured shifts in di-8-ANEPPS orientation. Using these results, r_c can be calculated for various values of p.

Assuming a pillar spacing of 36 nm, several parameters relating to the predicted change in membrane curvature can

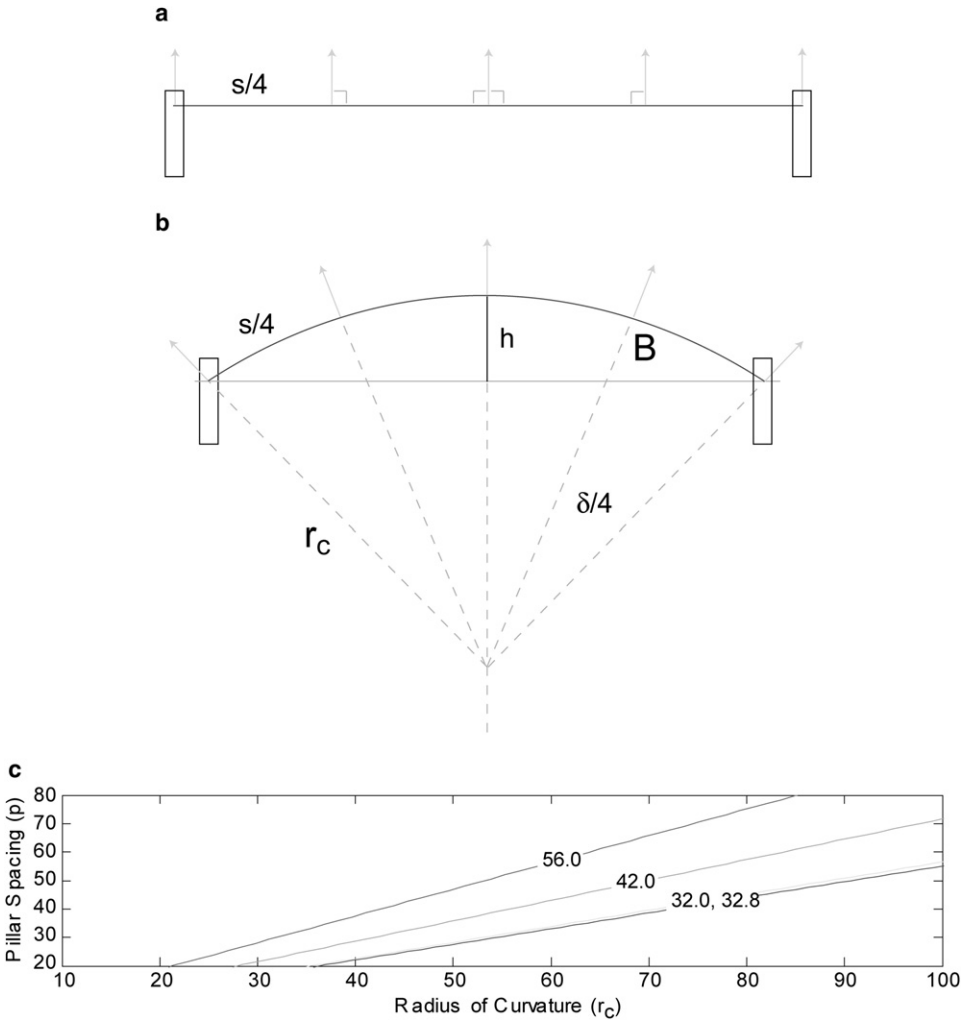

FIGURE 5 Graphical depiction of two-dimensional membrane deformation. (*a*) Membrane segment before deformation. The open black rectangles at either end represent the lateral wall pillar protein. Gray arrows indicate the approximate orientation of the emission transition dipole moment of di-8-ANEPPS. We assume for simplicity that di-8-ANEPPS molecules are evenly spaced along the membrane segment of arc length *s*. (*b*) Membrane segment following deformation. The average orientation of di-8-ANEPPS along the curved region of membrane is equivalent to the orientation of a single fluorophore at point B. The angle subtended by the segment of membrane is δ, and the corresponding radius of curvature is r_c. In this model we do not account for complex curvatures surely present at the intersection of the plasma membrane and each pillar protein. The new height of the membrane with respect to its initial location is designated as *h*. (*c*) Relationship between pillar spacing (*p*), radius of curvature (r_c), and the solid angle (δ). Curves are plotted over the relevant ranges of these parameters as defined by the literature and for the subtended angles corresponding to our measured shifts in di-8-ANEPPS orientation.

now be estimated (Table 2). These parameters include r_c, *s*, the height of the curved region of membrane in relation to a flat bilayer (*h*), and the surface area of the distended membrane region (SA_{tile}). We assume the OHC pillars maintain the same spacing circumferentially as axially. Extending the two-dimensional membrane bending shown in Fig. 5 into the third dimension, we allow only one radius of curvature approximating the membrane region spanning four pillars as a section of a cylinder (Fig. 6 *b*).

FPM experiments on di-8-ANEPPS-labeled, untreated OHCs predict the absorption transition dipole moment of di-8-ANEPPS to be oriented at ~30°. From previous studies, the angle between the absorption and emission transition dipole moments is known and is 62° (60), indicating the emission transition dipole moment orients at ~92°. This result suggests that there is very little or no initial curvature in the OHC membrane in isolated unclamped cells, a suggestion consistent with previous findings where cell shortening was seen following OHC treatment with either CPZ or TNP (17). If the OHC plasma membrane was initially curved, treatment with opposing amphipaths would result in length changes in opposite directions. Note, however, that the absence of initial curvature does not imply the absence of bending energy as the spontaneous curvature of the OHC plasma membrane is unknown.

With no initial curvature, the area of membrane spanning four pillar pinning points would simply be the area of a square with sides of 36 nm. Using this assumption, we can

TABLE 2 δ and r_c values corresponding to orientation shifts seen for treatment with 10 mM salicylate, 0.1 mM TNP, 0.1 mM CPZ, and 10 mM salicylate plus 0.1 mM CPZ

Treatment	$\Delta\theta$	δ	r_c (nm)	*s* (nm•rad)	*h* (nm)	SA_{tile} (nm^2)	Δ SA_{tile} (nm^2)
10 mM salicylate	11.4°	45.6°	46.4	36.9	3.6	1328.4	32.4
0.1 mM TNP	16.6°	66.4°	32.9	38.1	5.4	1371.6	75.6
0.1 mM CPZ	11.6°	46.4°	45.7	37.0	3.7	1332.0	36.0
10 mM salicylate + 0.1 mM CPZ	13.9°	55.6°	38.6	37.5	4.5	1350.0	54.0

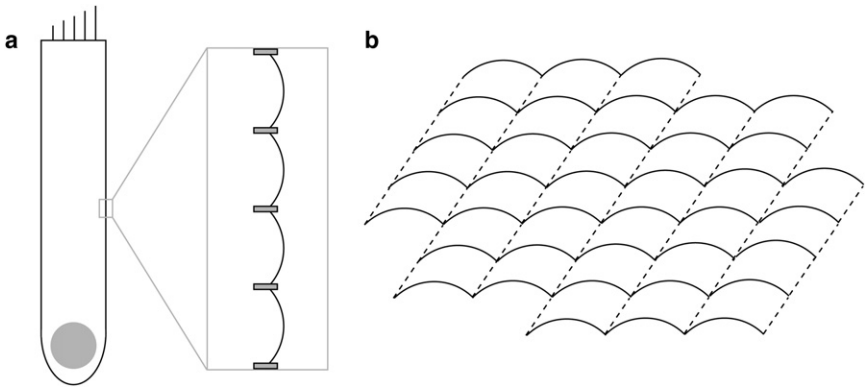

FIGURE 6 Graphical depiction of changes in membrane curvature at the cellular level. We assume constant pillar spacing in both the axial and circumferential directions. (*a*) OHC showing a close-up of the curved plasma membrane. Cytoskeletal pillar proteins act as anchors. (*b*) To simplify our curvature model, we assume that membrane bending occurs only at one radius of curvature in planes corresponding to the image plane. This image depicts a top-down view of the OHC membrane.

determine the fractional area change when the membrane bends (ΔSA_{tile}). The predicted changes in membrane height range from 3.6 to 5.4 nm, indicating subtle membrane bending, and the corresponding changes in membrane arc surface area range from 32 to 76 nm^2, a 2%–6% increase (Table 2). The curvature model demonstrated here reflects the lack of visible morphological OHC changes in response to amphipath partitioning, as nanoscale changes in membrane curvature would not be visible through light microscopy alone.

The relationship between observed shifts in di-8-ANEPPS orientation and predicted changes in OHC membrane curvature is further supported by the results from the simultaneous TNP and CPZ treatment. If each of these compounds' primary effect on OHCs is manifested as curvature changes induced via preferential partitioning, then simultaneous application at appropriate concentrations should result in no net membrane bending and therefore no shift in di-8-ANEPPS orientation. The orientation of di-8-ANEPPS in cells treated simultaneously with CPZ and TNP is 23.0°, a value that demonstrates CPZ and TNP's ability to attenuate each other's membrane-bending effects. The detectable, but insignificant orientation shift may arise from the use of CPZ and TNP concentrations that do not induce precisely equivalent membrane bending, a hypothesis that is supported by results from individual treatments. TNP induces a shift of 14°, whereas CPZ alters di-8-ANEPPS orientation by only 8.2°. Additionally, CPZ's inability to induce membrane bending as significant as TNPs may arise from the OHCs positive intracellular turgor pressure: inward membrane bending may be partially counteracted by this force.

Results from dual applications using salicylate are less straightforward. Treatment of OHCs with 10 mM salicylate and 0.1 mM CPZ simultaneously does not return di-8-ANEPPS to an orientation commensurate with untreated cells. Although salicylate has been shown to dramatically reduce the bending stiffness of synthetic membranes (71), salicylate also acts as a competitive antagonist to intracellular anions necessary for prestin function (64,65). As such, we consider two potential mechanisms for salicylate's effect on di-8-ANEPPS orientation: an effect mediated through membrane curvature and an effect mediated through interaction with prestin. Notably, at 0.5 mM, consistent trends in the data suggest that salicylate's effect on di-8-ANEPPS orientation may be partially attenuated by the simultaneous application of CPZ. Perhaps at lower concentrations where salicylate only slightly reduces prestin function, salicylate's membrane-mediated effects that shift the voltage sensitivity of the NLC are measurable. At the higher concentration of 10 mM, a sufficient amount of salicylate's charged species is present in the cytosol to either bind to or allosterically modulate prestin, resulting in greatly diminished function that masks the membrane-bending effects as a result of the reduction of the NLC curve.

Salicylate-prestin interactions

Our surprising observation that the orientation of di-8-ANEPPS remains shifted even after the application of CPZ to salicylate-treated OHCs suggests that in prestin's inhibited state, prestin-membrane interactions may significantly alter the material properties of the OHC bilayer. Perhaps the salicylate-induced conformational change in prestin elicits membrane bending? Alternatively, it is possible that the reversal of salicylate's bending effects at 10 mM may require a higher concentration of CPZ. However, in the simultaneous treatment, CPZ does not appear to even partially reverse the salicylate-induced di-8-ANEPPS orientation shift (Fig. 4). This result, combined with the evidence for an interaction between salicylate and prestin (64,65), advocates a more complicated mechanism for salicylate-induced prestin inhibition that would not be counteracted by higher concentrations of CPZ.

Implications for models of electromotility

Although our results provide evidence that the OHC plasma membrane is capable of bending in a manner originally predicted by the membrane-bending model of electromotility (38), they call into question some of the original assumptions of this model. The bending model assumed that units of OHC membrane between pillars were initially curved at the cell's holding potential. The observed shifts in

di-8-ANEPPS orientation following treatment with opposing amphipaths imply zero initial curvature, consistent with recent results demonstrating a shortening of OHCs following treatment with either CPZ or TNP (17). Although the initial curvature was mathematically introduced as an arbitrary parameter in the bending model (38), it is difficult to picture how electrically induced curvature deformations can both shorten and elongate the cell from a flat state without introducing additional complexity. Additionally, as recently discussed (17), evidence indicates that treatment with membrane altering agents does not necessarily disrupt electromotile force generation and that treatment with oppositely charged amphipaths shifts the voltage dependence of OHC NLC in the same direction. A more sophisticated model is needed to describe the relation between curvature elastic energy, prestin function, and the transmission of forces to the cytoskeleton.

A particular focus of future modeling efforts could distinguish the curvature sensitivity of prestin function from cellular motility and force generation. For example, if conformational changes of the motor protein drive or coincide with changes in membrane bending, treatment with agents known to affect membrane bending could conceivably shift the voltage sensitivity of prestin by inducing conformational changes without affecting the capacity for force generation. Under this picture, the bending of the OHC plasma membrane induced by CPZ or TNP could force more prestin molecules into the extended state, shifting the NLC curve in the positive direction. The capacity for force generation would remain intact, and the only change would be the relative distribution of motor proteins among possible states at the cell's normal holding potential.

CONCLUSION

The work presented here demonstrates the ability of FPM to measure subtle changes in membrane curvature. Our results indicate that CPZ and TNP are capable of inducing nanoscale curvature changes in the OHC plasma membrane that correlate with experimentally observed depolarizing shifts in NLC (15–17). For treatment with CPZ and TNP, these curvature changes are qualitatively explained by the predictions of the bilayer couple theory and are likely the mechanism by which these compounds alter the voltage dependence of prestin function (Fig. 7). This conclusion is consistent with previous suggestions that CPZ and TNP affect prestin function (17) and consequently cochlear amplification (73) in a membrane-mediated manner. Prestin's mechanosensitivity is intricately connected to alterations in bilayer properties since these changes affect the thermodynamic work required for conformational transitions and the generation of electromotile forces. Thus, the curvature, composition, and overall mechanics of the OHC plasma membrane must be held at a precise equilibrium point to optimize electromotility at physiological receptor potentials.

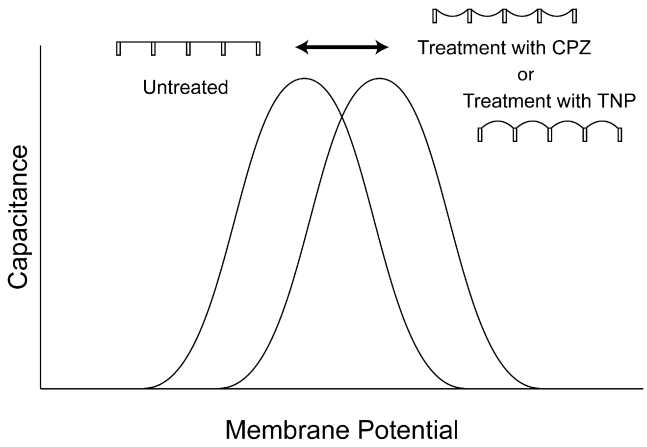

FIGURE 7 Depiction of NLC curve shifts correlating to changes in membrane bending. Both inward and outward bending induced by CPZ and TNP, respectively, induce similar depolarizing shifts in the peak of the NLC curve. For 0.1 mM CPZ, the shift is ~20 mV (16,17), and for 0.5 mM TNP, the shift is ~10 mV (17).

The authors thank Louise Organ, Fred Pereira, and Kuni Iwasa for thoughtful discussions, critiques, and manuscript comments and Eric Darling for assistance with statistical analyses.

This work was supported by a National Institutes of Health/National Institute on Deafness and Other Communication Disorders National Research Service Award Predoctoral Fellowship (to J.N.G., DC07563-01), a National Organization for Hearing Research Foundation Grant (to R.M.R.), a National Science Foundation Career Award (to R.M.R., BES 0449379), and a National Institutes of Health/National Institute on Deafness and Other Communication Disorders R21 (DC008134).

REFERENCES

1. Brownell, W. E., C. R. Bader, D. Bertrand, and Y. de Ribaupierre. 1985. Evoked mechanical responses of isolated cochlear outer hair cells. *Science*. 227:194–196.
2. Kachar, B., W. E. Brownell, R. Altschuler, and J. Fex. 1986. Electrokinetic shape changes of cochlear outer hair cells. *Nature*. 322:365–368.
3. Ashmore, J. F. 1987. A fast motile response in guinea-pig outer hair cells: the cellular basis of the cochlear amplifier. *J. Physiol.* 388:323–347.
4. Spector, A. A., N. Deo, K. Grosh, J. T. Ratnanather, and R. M. Raphael. 2006. Electromechanical models of the outer hair cell composite membrane. *J. Membr. Biol.* 209:135–152.
5. Brownell, W. E., A. A. Spector, R. M. Raphael, and A. S. Popel. 2001. Micro- and nanomechanics of the cochlear outer hair cell. *Annu. Rev. Biomed. Eng.* 3:169–194.
6. Liberman, M. C., J. Gao, D. Z. He, X. Wu, S. Jia, and J. Zuo. 2002. Prestin is required for electromotility of the outer hair cell and for the cochlear amplifier. *Nature*. 419:300–304.
7. He, D. Z., J. Zheng, F. Kalinec, S. Kakehata, and J. Santos-Sacchi. 2006. Tuning in to the amazing outer hair cell: membrane wizardry with a twist and shout. *J. Membr. Biol.* 209:119–134.
8. Ashmore, J. F. 1990. Forward and reverse transduction in the mammalian cochlea. *Neurosci. Res. Suppl.* 12:S39–S50.
9. Santos-Sacchi, J. 1991. Reversible inhibition of voltage-dependent outer hair cell motility and capacitance. *J. Neurosci.* 11:3096–3110.
10. Dallos, P., and B. Fakler. 2002. Prestin, a new type of motor protein. *Nat. Rev. Mol. Cell Biol.* 3:104–111.

11. Kakehata, S., and J. Santos-Sacchi. 1995. Membrane tension directly shifts voltage dependence of outer hair cell motility and associated gating charge. *Biophys. J.* 68:2190–2197.
12. Sturm, A. K., L. Rajagopalan, D. Yoo, W. E. Brownell, and F. A. Pereira. 2007. Functional expression and microdomain localization of prestin in cultured cells. *Otolaryngol. Head Neck Surg.* 136:434–439.
13. Rajagopalan, L., J. N. Greeson, A. Xia, H. Liu, A. Sturm, et al. 2007. Tuning of the outer hair cell motor by membrane cholesterol. *J. Biol. Chem.* 282:36659–36670.
14. Tunstall, M. J., J. E. Gale, and J. F. Ashmore. 1995. Action of salicylate on membrane capacitance of outer hair cells from the guinea-pig cochlea. *J. Physiol.* 485:739–752.
15. Kakehata, S., and J. Santos-Sacchi. 1996. Effects of salicylate and lanthanides on outer hair cell motility and associated gating charge. *J. Neurosci.* 16:4881–4889.
16. Lue, A. J., H. B. Zhao, and W. E. Brownell. 2001. Chlorpromazine alters outer hair cell electromotility. *Otolaryngol. Head Neck Surg.* 125:71–76.
17. Fang, J., and K. H. Iwasa. 2007. Effects of chlorpromazine and trinitrophenol on the membrane motor of outer hair cells. *Biophys. J.* 93:1809–1817.
18. Shehata, W. E., W. E. Brownell, and R. Dieler. 1991. Effects of salicylate on shape, electromotility and membrane characteristics of isolated outer hair cells from guinea pig cochlea. *Acta Otolaryngol.* 111:707–718.
19. Oghalai, J. S., H. B. Zhao, J. W. Kutz, and W. E. Brownell. 2000. Voltage- and tension-dependent lipid mobility in the outer hair cell plasma membrane. *Science.* 287:658–661.
20. Murdock, D. R., S. A. Ermilov, A. A. Spector, A. S. Popel, W. E. Brownell, et al. 2005. Effects of chlorpromazine on mechanical properties of the outer hair cell plasma membrane. *Biophys. J.* 89:4090–4095.
21. Ermilov, S. A., D. R. Murdock, D. El-Daye, W. E. Brownell, and B. Anvari. 2005. Effects of salicylate on plasma membrane mechanics. *J. Neurophysiol.* 94:2105–2110.
22. Oghalai, J. S. 2004. Chlorpromazine inhibits cochlear function in guinea pigs. *Hear. Res.* 198:59–68.
23. Sheetz, M. P., R. G. Painter, and S. J. Singer. 1976. Biological membranes as bilayer couples. III. Compensatory shape changes induced in membranes. *J. Cell Biol.* 70:193–203.
24. Sheetz, M. P., and S. J. Singer. 1974. Biological membranes as bilayer couples. A molecular mechanism of drug-erythrocyte interactions. *Proc. Natl. Acad. Sci. USA.* 71:4457–4461.
25. Sheetz, M. P., and S. J. Singer. 1976. Equilibrium and kinetic effects of drugs on the shapes of human erythrocytes. *J. Cell Biol.* 70:247–251.
26. Deuticke, B. 1968. Transformation and restoration of biconcave shape of human erythrocytes induced by amphiphilic agents and changes of ionic environment. *Biochim. Biophys. Acta.* 163:494–500.
27. Evans, E. A. 1974. Bending resistance and chemically induced moments in membrane bilayers. *Biophys. J.* 14:923–931.
28. Svetina, S., and B. Zeks. 1989. Membrane bending energy and shape determination of phospholipid vesicles and red blood cells. *Eur. Biophys. J.* 17:101–111.
29. Lim, H. W. G., M. Wortis, and R. Mukhopadhyay. 2002. Stomatocyte-discocyte-echinocyte sequence of the human red blood cell: evidence for the bilayer-couple hypothesis from membrane mechanics. *Proc. Natl. Acad. Sci. USA.* 99:16766–16769.
30. Derganc, J., B. Bozic, S. Svetina, and B. Zeks. 2003. Equilibrium shapes of erythrocytes in rouleau formation. *Biophys. J.* 84:1486–1492.
31. Zheng, J., W. Shen, D. Z. He, K. B. Long, L. D. Madison, et al. 2000. Prestin is the motor protein of cochlear outer hair cells. *Nature.* 405:149–155.
32. Mount, D. B., and M. F. Romero. 2004. The SLC26 gene family of multifunctional anion exchangers. *Pflugers Arch.* 447:710–721.
33. Belyantseva, I. A., H. J. Adler, R. Curi, G. I. Frolenkov, and B. Kachar. 2000. Expression and localization of prestin and the sugar transporter GLUT-5 during development of electromotility in cochlear outer hair cells. *J. Neurosci.* 20:RC116.
34. Kalinec, F., M. C. Holley, K. H. Iwasa, D. J. Lim, and B. Kachar. 1992. A membrane-based force generation mechanism in auditory sensory cells. *Proc. Natl. Acad. Sci. USA.* 89:8671–8675.
35. Santos-Sacchi, J. 1993. Harmonics of outer hair cell motility. *Biophys. J.* 65:2217–2227.
36. Dallos, P., R. Hallworth, and B. N. Evans. 1993. Theory of electrically driven shape changes of cochlear outer hair cells. *J. Neurophysiol.* 70:299–323.
37. Iwasa, K. H. 1994. A membrane motor model for the fast motility of the outer hair cell. *J. Acoust. Soc. Am.* 96:2216–2224.
38. Raphael, R. M., A. S. Popel, and W. E. Brownell. 2000. A membrane bending model of outer hair cell electromotility. *Biophys. J.* 78:2844–2862.
39. Andersen, O. S., and Koeppe, R.E. 2nd. 2007. Bilayer thickness and membrane protein function: an energetic perspective. *Annu. Rev. Biophys. Biomol. Struct.* 36:107–130.
40. Martinac, B., J. Adler, and C. Kung. 1990. Mechanosensitive ion channels of *E. coli* activated by amphipaths. *Nature.* 348:261–263.
41. Kung, C. 2005. A possible unifying principle for mechanosensation. *Nature.* 436:647–654.
42. Brown, M. F. 1994. Modulation of rhodopsin function by properties of the membrane bilayer. *Chem. Phys. Lipids.* 73:159–180.
43. Park, J. B., H. J. Kim, P. D. Ryu, and E. Moczydlowski. 2003. Effect of phosphatidylserine on unitary conductance and Ba^{2+} block of the BK Ca^{2+}-activated K^+ channel: re-examination of the surface charge hypothesis. *J. Gen. Physiol.* 121:375–397.
44. Chang, H. M., R. Reitstetter, and R. Gruener. 1995. Lipid-ion channel interactions: increasing phospholipid headgroup size but not ordering acyl chains alters reconstituted channel behavior. *J. Membr. Biol.* 145:13–19.
45. Kim, K. S., J. Neu, and G. Oster. 1998. Curvature-mediated interactions between membrane proteins. *Biophys. J.* 75:2274–2291.
46. Botelho, A. V., T. Huber, T. P. Sakmar, and M. F. Brown. 2006. Curvature and hydrophobic forces drive oligomerization and modulate activity of rhodopsin in membranes. *Biophys. J.* 91:4464–4477.
47. Navaratnam, D., J. P. Bai, H. Samaranayake, and J. Santos-Sacchi. 2005. N-terminal-mediated homomultimerization of prestin, the outer hair cell motor protein. *Biophys. J.* 89:3345–3352.
48. Greeson, J. N., L. E. Organ, F. A. Pereira, and R. M. Raphael. 2006. Assessment of prestin self-association using fluorescence resonance energy transfer. *Brain Res.* 1091:140–150.
49. Zheng, J., G. G. Du, C. T. Anderson, J. P. Keller, A. Orem, et al. 2006. Analysis of the oligomeric structure of the motor protein prestin. *J. Biol. Chem.* 281:19916–19924.
50. Wu, X., B. Currall, T. Yamashita, L. L. Parker, R. Hallworth, et al. 2007. Prestin-prestin and prestin-GLUT5 interactions in HEK293T cells. *Dev. Neurobiol.* 67:483–497.
51. Cantor, R. S. 1997. The lateral pressure profile in membranes: a physical mechanism of general anesthesia. *Biochemistry.* 36:2339–2344.
52. Cantor, R. S. 1997. Lateral pressures in cell membranes: a mechanism for modulation of protein function. *J. Phys. Chem.* 101:1723–1725.
53. Cantor, R. S. 1998. The lateral pressure profile in membranes: a physical mechanism of general anesthesia. *Toxicol. Lett.* 100–101:451–458.
54. Cantor, R. S. 1999. Lipid composition and the lateral pressure profile in bilayers. *Biophys. J.* 76:2625–2639.
55. Cantor, R. S. 1999. The influence of membrane lateral pressures on simple geometric models of protein conformational equilibria. *Chem. Phys. Lipids.* 101:45–56.
56. Mio, K., Y. Kubo, T. Ogura, T. Yamamoto, F. Arisaka, et al. 2007. The motor protein prestin is a bullet-shaped molecule with inner cavities. *J. Biol. Chem.* 283:1137–1145.
57. Holley, M. C., and J. F. Ashmore. 1990. Spectrin, actin and the structure of the cortical lattice in mammalian cochlear outer hair cells. *J. Cell Sci.* 96:283–291.
58. Holley, M. C., F. Kalinec, and B. Kachar. 1992. Structure of the cortical cytoskeleton in mammalian outer hair cells. *J. Cell Sci.* 102:569–580.

59. Zhi, M., J. T. Ratnanather, E. Ceyhan, A. S. Popel, and W. E. Brownell. 2007. Hypotonic swelling of salicylate-treated cochlear outer hair cells. *Hear. Res.* 228:95–104.

60. Greeson, J. N., and R. M. Raphael. 2007. Application of fluorescence polarization microscopy to measure fluorophore orientation in the outer hair cell plasma membrane. *J. Biomed. Opt.* 12:021002.

61. Axelrod, D. 1979. Carbocyanine dye orientation in red cell membrane studied by microscopic fluorescence polarization. *Biophys. J.* 26:557–573.

62. Fluhler, E., V. G. Burnham, and L. M. Loew. 1985. Spectra, membrane binding, and potentiometric responses of new charge shift probes. *Biochemistry.* 24:5749–5755.

63. Loew, L. M. 1996. Potentiometric dyes: imaging electrical activity of cell membranes. *Pure Appl. Chem.* 68:1405–1409.

64. Oliver, D., D. Z. He, N. Klèocker, J. Ludwig, U. Schulte, et al. 2001. Intracellular anions as the voltage sensor of prestin, the outer hair cell motor protein. *Science.* 292:2340–2343.

65. Santos-Sacchi, J., L. Song, J. Zheng, and A. L. Nuttall. 2006. Control of mammalian cochlear amplification by chloride anions. *J. Neurosci.* 26:3992–3998.

66. Oghalai, J. S., A. A. Patel, T. Nakagawa, and W. E. Brownell. 1998. Fluorescence-imaged microdeformation of the outer hair cell lateral wall. *J. Neurosci.* 18:48–58.

67. Oghalai, J. S., T. D. Tran, R. M. Raphael, T. Nakagawa, and W. E. Brownell. 1999. Transverse and lateral mobility in outer hair cell lateral wall membranes. *Hear. Res.* 135:19–28.

68. de Monvel, J. B., W. E. Brownell, and M. Ulfendahl. 2006. Lateral diffusion anisotropy and membrane lipid/skeleton interaction in outer hair cells. *Biophys. J.* 91:364–381.

69. Greeson, J.N. 2008. Investigating the role of the outer hair cell plasma membrane in electromotility and prestin function using quantitative optical microscopy techniques. *In* Bioengineering. Rice University, Houston, TX.

70. Greeson, J. N., and R. M. Raphael. 2005. Orientation of membrane probes in giant unilamellar vesicles. *Proc. SPIE.* 5699:211–218.

71. Zhou, Y., and R. M. Raphael. 2005. Effect of salicylate on the elasticity, bending stiffness, and strength of SOPC membranes. *Biophys. J.* 89:1789–1801.

72. Forge, A. 1991. Structural features of the lateral walls in mammalian cochlear outer hair cells. *Cell Tissue Res.* 265:473–483.

73. Zheng, J., N. Deo, Y. Zou, K. Grosh, and A. L. Nuttall. 2007. Chlorpromazine alters cochlear mechanics and amplification: in vivo evidence for a role of stiffness modulation in the organ of corti. *J. Neurophysiol.* 97:994–1004.